IEEE Photonics Journal
An IEEE Photonics Society Publication

Optical OFDM Synchronization With Symbol Timing Offset and Sampling Clock Offset Compensation in Real-Time IMDD Systems

Volume 3, Number 2, April 2011

X. Q. Jin
J. M. Tang

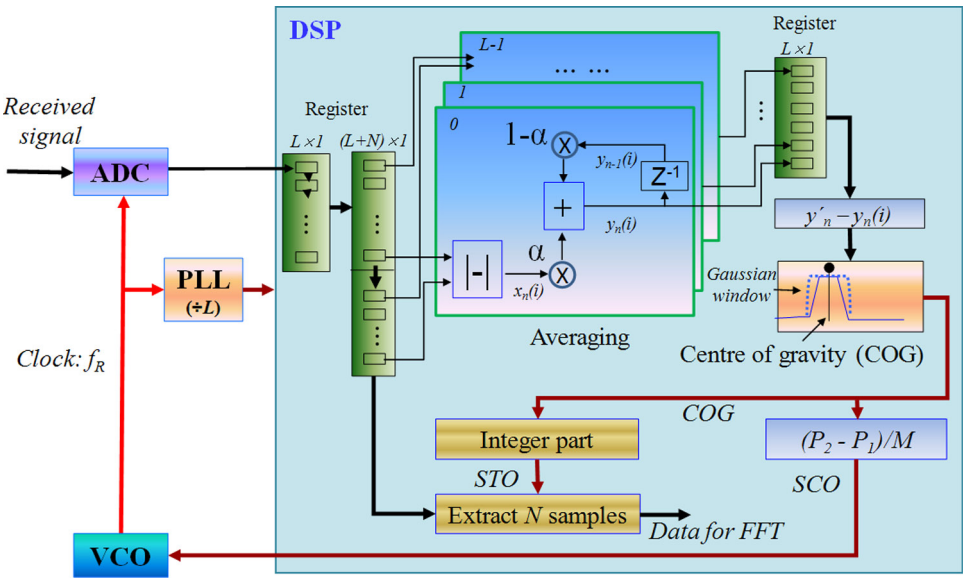

DOI: 10.1109/JPHOT.2011.2120602
1943-0655/$26.00 ©2011 IEEE

Optical OFDM Synchronization With Symbol Timing Offset and Sampling Clock Offset Compensation in Real-Time IMDD Systems

X. Q. Jin and J. M. Tang

School of Electrical Engineering, Bangor University, Bangor LL57 1UT U.K.

DOI: 10.1109/JPHOT.2011.2120602
1943-0655/$26.00 ©2011 IEEE

Manuscript received February 5, 2011; revised February 22, 2011; accepted February 22, 2011. Date of publication February 28, 2011; date of current version March 11, 2011. Corresponding author: X. Q. Jin (e-mail: x.jin@bangor.ac.uk).

Abstract: End-to-end real-time Optical Orthogonal Frequency Division Multiplexing (OOFDM) signal synchronization that is capable of simultaneously compensating for both Symbol Timing Offset (STO) and Sampling Clock Offset (SCO) is experimentally demonstrated, for the first time, over 64-quadrature amplitude modulated (QAM)-encoded, 11.25-Gb/s, 25-km, Intensity-Modulation and Direct-Detection (IMDD) single mode fiber (SMF) systems employing directly modulated distributed feedback lasers. In comparison with manual synchronization, almost-perfect compensations of arbitrary STOs are achieved. The OOFDM synchronization technique can also compensate for the SCO effect with an accuracy of < 1 ppm for initial SCOs as large as 4000 ppm. The technique has a number of salient advantages including low complexity, fast tracking speed, high accuracy, and suitability for high-speed optical transmission systems.

Index Terms: Fiber optics systems, synchronization, optical modulation, orthogonal frequency division multiplexing (OFDM).

1. Introduction

The realization of high-speed, low-complexity, Optical Orthogonal Frequency Division Multiplexing (OOFDM) synchronization with excellent accuracy is extremely vital for implementation of the OOFDM technique in cost-effective, next-generation, high-capacity transmission systems [1]. Generally speaking, for any transmission systems, there are two distinct receiver clock generation approaches: asynchronous and synchronous. In an asynchronously clocked system, the receiver operates with an independent clock and uses the received signal to accurately detect the offset between the transmitter and receiver clocks; the offset effects are then compensated in the receiver, while in a synchronously clocked system, the receiver extracts a synchronous clock signal from the received signal based on embedded timing information [1].

For asynchronously clocked, Intensity-Modulation and Direct-Detection (IMDD) OOFDM transmission systems of interest of the present paper, Symbol Timing Offset (STO) and Sampling Clock Offset (SCO) play dominant roles in determining the achievable system performance [2]. STO and SCO occur due to the time delay of a transmission link and the clock mismatch between the transmitter and the receiver, respectively. A STO-induced synchronization error may cause a fraction of a Fast Fourier Transform (FFT) window to occur in an extended region of an adjacent symbol, leading to system performance degradation. On the other hand, SCO causes not only the drift in symbol timing but the significant Inter-Carrier Interference (ICI) effect as well as the sampled

value does not correspond to the maximum value of the OOFDM subcarrier spectrum $[sin(x)/x]$ after the FFT in the receiver.

The experimental explorations of asynchronous OOFDM synchronization have been undertaken using both offline Digital Signal Processing (DSP) [3]–[5] and real-time DSP [2], [6], [7]. Clearly, offline DSP synchronization [3]–[5] does not consider the limitations imposed by the precision and speed of practical DSP hardware required for realizing real-time high-speed OOFDM systems. While real-time DSP-based OOFDM synchronization [6], [7] has been experimentally demonstrated using approaches similar to those adopted in wireless systems [8]–[10], where training symbols are transmitted once every certain number of symbols and correlation operations are applied to the received training symbols to recover the clock, the latter approach has, however, not been experimentally achieved in end-to-end real-time OOFDM systems and occupies the valuable transmission bandwidth. In addition, the compensation of the SCO effect is not considered, as a common clock for the transmitter and receiver is employed.

Given the fact that optical fiber channels are of improved stability compared with wireless systems, OOFDM synchronization does not have to take place very frequently. In addition, the insertion of a Cyclic Prefix (CP) to each symbol brings about a repeated OOFDM symbol pattern with a predetermined time period. Thus, full use can be made of the aforementioned features to significantly reduce the complexity of OOFDM synchronization in asynchronously clocked IMDD systems. A novel CP-based OOFDM synchronization technique was proposed by using the subtraction operation instead of the conjugate multiplication operation [2]. The main advantages of the technique are low complexity, suitability for high-speed transmission, and bandwidth occupation free. The OOFDM synchronization technique with STO compensation has been experimentally demonstrated in 6.56-Gb/s, 25-km IMDD systems using a common clock for both the transmitter and receiver [2].

Here, it is worth pointing out that, in wireless OFDM systems, CP-based OFDM synchronization has also been reported [11]–[14], where a sophisticated maximum likelihood estimator based on the log-likelihood function is adopted to compensate the STO and/or SCO effects. In addition, conjugate multiplication [8]–[14] is required, and computation of inverse tangent is utilized to identify phase information [8], [9], [11]–[14]. Clearly, this significantly increases the complexity of DSP design. Furthermore, as commercially available DSP units can only operate at speeds much lower than sampling speeds of Analog-to-Digital Converters (ADCs), parallel signal processing is thus required to enable the implementation of the technique in high-speed systems ($>$ 10 Gb/s). Obviously, high-speed parallel signal processing requires more multiplication and/or addition operations, thus leading to a further increase in system complexity. Therefore, the conventional CP-based OFDM synchronization technique may not be suitable for end-to-end real-time, high-speed OOFDM systems.

In this paper, in an asynchronously locked OOFDM IMDD system using independent clocks for the transmitter and receiver, the performance of the previously reported OOFDM synchronization technique [2] is significantly improved in terms of the following two crucial aspects: 1) In addition to accurate STO compensation, SCO compensation is also achieved, for the first time, with an accuracy of $<$ 1 ppm for initial SCOs as large as 4000 ppm; 2) such complete synchronization with both STO and SCO compensation operates at higher signal bit rates of 11.25 Gb/s and a three-times lower total channel bit error rate (BER) as well as a $>$ 3-dB improvement in optical power budget. The present work strongly confirms that the synchronization technique is of low complexity, fast tracking speed, high accuracy, and suitability for high-speed optical transmission.

2. OOFDM Synchronization Principle

As detailed descriptions of the OOFDM synchronization operating principles have been reported in [2], here, brief discussions of the technique are presented for the integrity of the present paper. Fig. 1 shows the conceptual diagram of the synchronization technique that are capable of compensating for both the STO and SCO effects.

As seen in Fig. 1, in the receiver, a received real-valued digital OFDM sample sequence is first truncated and subsequently converted from serial to parallel, and each of the parallel sample

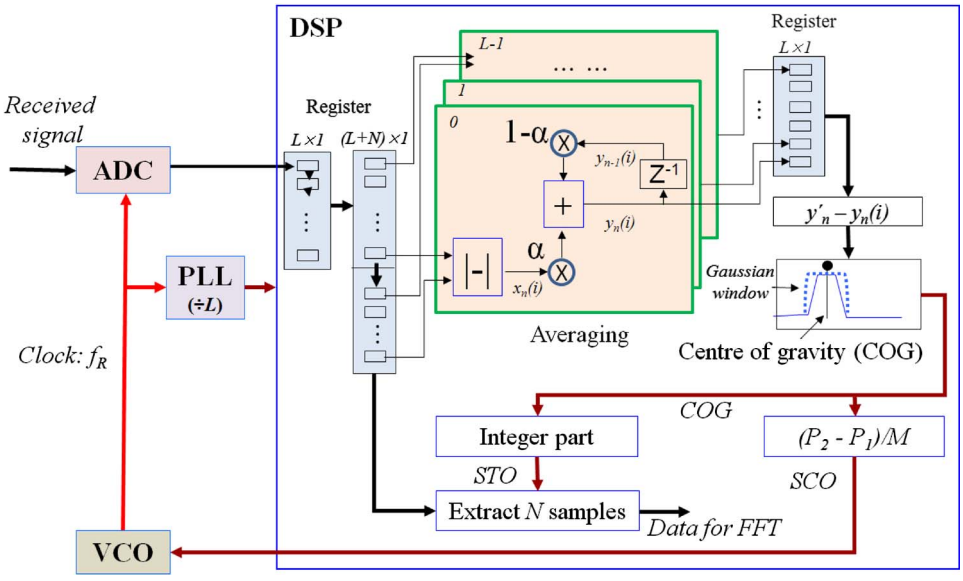

Fig. 1. Diagram of the demonstrated synchronization technique. VCO: voltage control oscillator. PLL: phase-locked loop. L: OOFDM symbol length, N: FFT window length. y'_n is the maximum value within $y_n(i)$. Z^{-1}: one-symbol delay.

groups contains L consecutive samples with L being the symbol length. After that, a sample group having $(L+N)$ samples is produced by copying a part (N samples) of the previously stored L samples into another register. Here, N is the Inverse Fast Fourier Transform (IFFT)/FFT window length. The captured nth sample group is denoted as $r_n(i^*), i^* = 0, 1, 2, \ldots, L+N-1$. At the symbol rate, an un-averaged synchronization profile $x_n(i)$ is generated by performing L parallel subtraction operations described as

$$x_n(i) = |r_n(i) - r_n(i+N)|, \quad i = 0, 1, 2, \ldots, L-1. \tag{1}$$

As the sample amplitudes are random in the FFT/IFFT window region, and the repeated sample patterns occur only in the CP region, the exact value of $x_n(i)$ in (1) depends upon whether the sample i locates in the CP region or not; if the sample at i locates in the CP region, its value is very similar to that corresponding to the sample at $(i+N)$. Thus, $x_n(i)$ approaches zero. Of course, slight deviations from zero may occur from symbol to symbol due to system random noise as well as ICI and Inter-Symbol-Interference (ISI); on the other hand, if the sample at i does not belong to the CP region, $x_n(i)$ has a random value, which varies from sample to sample and from symbol to symbol.

To effectively reduce the aforementioned random synchronization profile variations and the ISI effect, an average operation continuously accumulated over all the previously obtained un-averaged synchronization profiles is performed by

$$y_n(i) = \alpha x_n(i) + (1-\alpha) y_{n-1}(i) \tag{2}$$

where $y_n(i)$ is the synchronization profile vector in the register, and $y_0(i) = 0$. α is the coefficient, which controls the growth of $y_n(i)$. After averaging, $y_n(i)$ has a minimum value in the CP region.

To further improve the accuracy of the synchronization profile $y_n(i)$, the residual random variations of $y_n(i)$ outside the CP region should be reduced. To achieve such a goal, Gaussian windowing is introduced in the CP region by multiplying the inversed synchronization profile and a Gaussian window function [2]. After the Gaussian windowing operation, the obtained synchronization profile in the CP region can be well preserved, while the random $y_n(i)$ variation outside the CP region is significantly reduced. The final synchronization profile is then used for STO and SCO estimation and compensation.

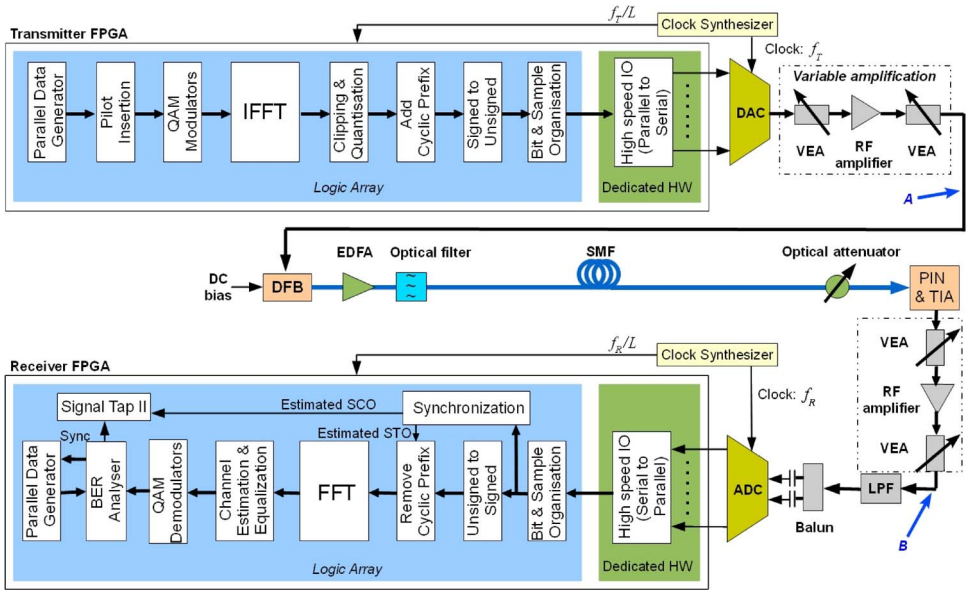

Fig. 2. End-to-end real-time experimental OOFDM system setup with synchronization. VEA: variable electrical attenuator. LPF: low-pass filter.

The Center Of Gravity (COG) is defined as the position that divides the synchronization profile into two equal areas. The integer part of the COG is used to mark the starting point of an FFT window, thus leading to the accurate compensation of the STO effect. The COG can also be utilized to trace the SCO effect. For IMDD transmission systems, a COG variation is proportional to SCO [2] by measuring two COGs P_1 and P_2 at different times, and the SCO ξ can be estimated by

$$\xi = (P_2 - P_1)/M \tag{3}$$

where M is the total number of samples during the time interval for measuring P_1 and P_2. ξ can be used to generate a synchronization signal to control and lock, via a Voltage Control Oscillator (VCO), the frequency of the receiver clock to compensate for the SCO effect.

It should be noted that, in implementing Gaussian windowing, the center of the Gaussian window is chosen to be the COG when the distance between the COG and the resulting synchronization profile peak is less than the CP period. Beyond such a regime, the Gaussian window center is taken to be the synchronization profile peak [2].

3. End-to-End Real-Time OOFDM Systems With Synchronization

Fig. 2 illustrates the end-to-end real-time Directly Modulated Distributed Feedback Laser (DML)-based, 25-km MetroCor single mode fiber (SMF) IMDD OOFDM system with synchronization. The real-time 64-quadrature amplitude modulated (QAM)-encoded 11.25-Gb/s OOFDM transceiver architectures, channel estimation and equalization, adaptive power loading, live parameter control, and on-line performance analysis functions are similar to those reported in [15], except that two separate clock synthesizers are utilized in Fig. 2 to generate independent clocks for the transmitter and receiver. A number of α values are stored in the memory of the field-programmable gate array and can be selected via a Joint Test Action Group connection to a PC. The corresponding component and system parameters utilized in Fig. 2 are identical to those presented in [2], except that the Digital-to-Analog Converter (DAC)/ADC with 8-bit resolution operates at a sampling speed of 4 GS/s. The symbol length is 40 samples (10 ns), and the CP length is 8 samples (2 ns). An optimum Gaussian window width of 1.3 times larger than the CP period is employed, which is identical to that reported in [2]. The DML driving voltage is approximately 0.4 Vpp, and the bias current is 36 mA,

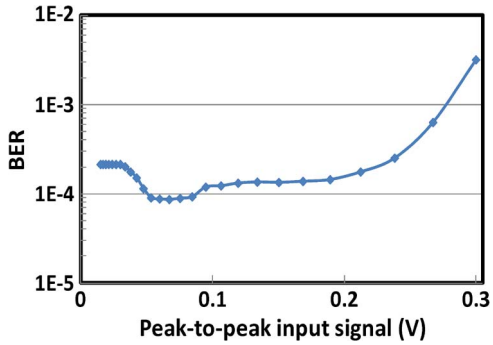

Fig. 3. Total channel BER performance versus peak-to-peak of the signal input to the radio frequency amplifier in the electrical back-to-back system configuration.

corresponding to the optical output power being −3.5 dBm. The optical powers injected into the MetroCor SMFs are fixed at 7 dBm.

4. Experimental Results

4.1. Electrical Signal Peak-to-Peak (PTP) Value Optimization

To overcome the imperfection of the radio frequency (RF) amplifier transfer function, the PTP value of the electrical OFDM signal input to the RF amplifier is first optimized in an electrical back-to-back system configuration, where point A in the transmitter is directly connected to point B in the receiver, as shown in Fig. 2. By taking the amplified electrical OFDM signal at an optimum level corresponding to the receiver ADC to fix the quantization noise effect, Fig. 3 is plotted to show the measured total channel BER as a function of PTP of the 64-QAM-encoded input OFDM signal with adaptive power loading [1]. An optimum input signal PTP range of 0.05 $\sim$ 0.09 V is experimentally observed, below which the BER reduction with increasing PTP is because of the increased PTP-induced growth in effective signal SNR. While, for signal PTPs of $>$ 0.09 V, a BER increase with increasing PTP occurs due to the electrical signal starts to penetrate into the nonlinear region of the RF amplifier, clearly, the optimum input signal PTP range is determined by the RF amplifier and the DAC/ADC. The identified optimum PTP value of 0.07 V is utilized in all the following experimental measurements.

4.2. STO Compensation

Fig. 4(a) shows the measured synchronization profiles for an initial SCO of 0 ppm in an 11.25-Gb/s 25-km MetroCor SMF IMDD system. As seen in Fig. 4(a), Gaussian windowing can significantly reduce the residual random synchronization profile variations outside the CP region and thus improve the synchronization accuracy. This statement can be understood by considering Fig. 4(b), where the dynamic COG evolution for an initial SCO of 0 ppm is presented. In obtaining Fig. 4(b), an extra 8-sample delay is inserted into a normally running synchronized transmission system. Fig. 4(c) shows the measured COGs for different α. It can be seen in Fig. 4(c) that, for a small α value, the COG variation is small, indicating that a small α value is preferred for obtaining a stable COG. However, a small value of α gives rise to a slow SCO tracking speed, as discussed in Section 4.3.

To explicitly demonstrate the effectiveness of the synchronization technique in compensating for the STO effect, Fig. 5 is shown, in which the measured total channel BER is plotted as a function of FFT window offset within the CP region for a system similar to that used in Fig. 4. The zero FFT window offset in Fig. 5 corresponds to the position achieved using the synchronization technique. The occurrence of the minimum BER at the zero offset position confirms that the synchronization technique can accurately and efficiently compensate for the STO effect.

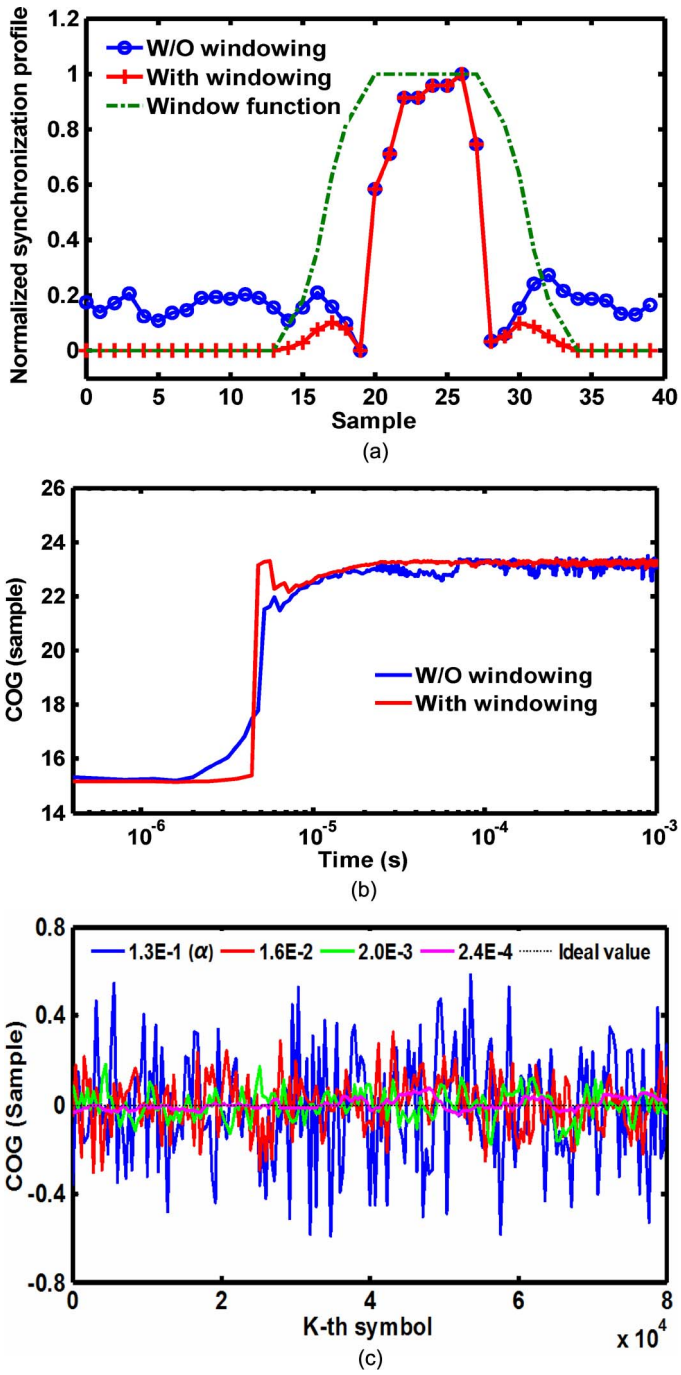

Fig. 4. (a) Normalized synchronization profile and (b) dynamic COG evolution with/without Gaussian windowing (SCO: 0 ppm, $\alpha : 2 \times 10^{-3}$). (c) Dynamic COG evolution for different α values at an initial SCO of 0 ppm.

4.3. SCO Compensation

To explore the capability of the synchronization technique in accurately tracking the SCO effect, for different α parameters, the SCO estimated by the technique versus the SCO introduced at the start of the communication session is plotted in Fig. 6(a). It is shown that the estimated SCO is identical to the real SCO values of up to 4000 ppm when $\alpha > 1.6 \times 10^{-2}$. This indicates that the

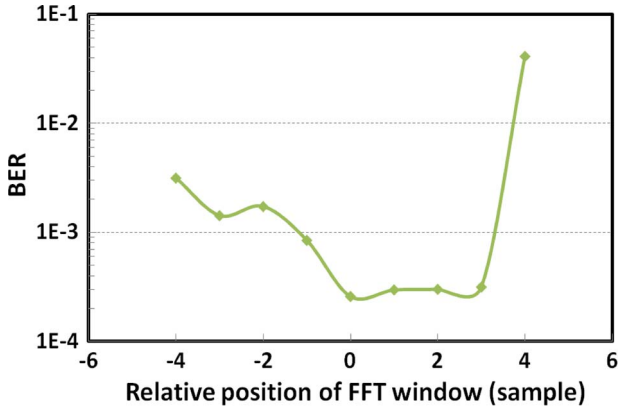

Fig. 5. Total channel BER performance versus relative FFT window position in 11.25-Gb/s 25-km MetroCor SMF systems (SCO: 0 ppm, $\alpha : 2 \times 10^{-3}$).

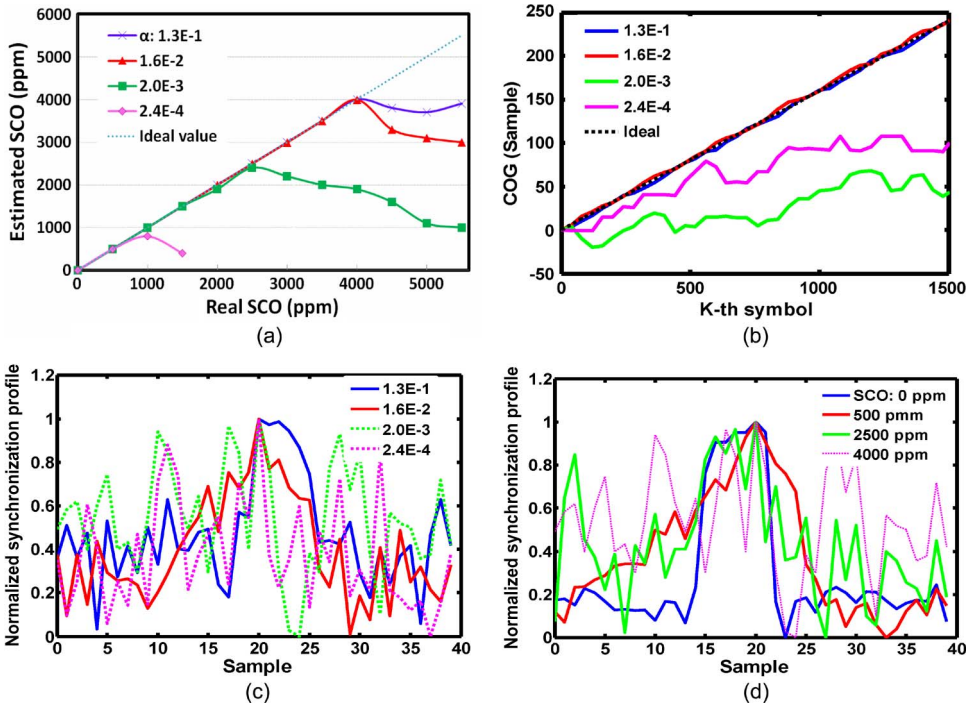

Fig. 6. (a) SCO tracking performance in an 11.25-Gb/s 25-km SMF transmission system, (b) dynamic COG evolution for a SCO of 4000 ppm, (c) normalized synchronization profile prior to applying Gaussian windowing for different α values (SCO: 4000 ppm), and (d) different SCO $(\alpha : 2 \times 10^{-3})$.

technique can accommodate a large SCO for a large α. For a small α, the maximum SCO value that the technique can accommodate becomes smaller, as shown in Fig. 6(a). This is because a small α value lowers the COG tracking speed, thus degrading the SCO estimation accuracy. The relationships between COG and α are presented in Fig. 6(b), which shows that the COG for a small α differentiates from an ideal COG for the following two reasons: 1) a slow tracking speed for a small α causes the relatively noisy synchronization profiles for the time period considered, as seen in Fig. 6(c); and 2) for a fixed α, the synchronization profile corresponding to a large SCO is

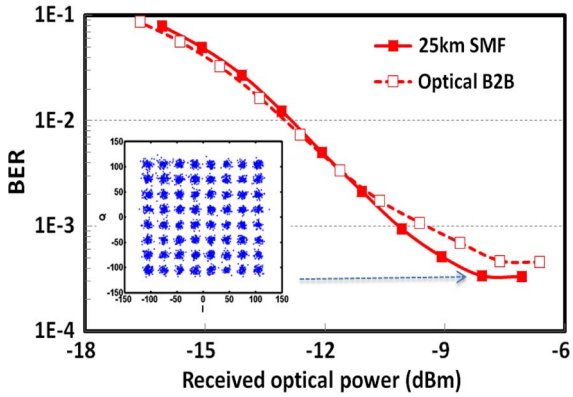

Fig. 7. Total channel BER versus received optical power at an initial SCO of 0 ppm ($\alpha : 2 \times 10^{-3}$).

TABLE 1

Complexity Comparisons. *L*: Symbol Length of 40 Samples (Including the CP), N_C: Eight CP Samples. Number of arg(•): Number of Computations for Inverse Tangent

Complexity	Multiplication	Addition	Number of arg(·)
Proposed synchronization	2L+2	4L+2	0
CP-based synchronization [11-13]	5L	$(3N_C-2)L$	1
Training-sequence-based synchronization [9]	3L	$(N_C+1)L$	2

broadened compared to that for a small SCO, as seen in Fig. 6(d). It is also necessary to mention that the accuracy of the estimated SCO is <1 ppm when SCO is close to 0 ppm. Considering the tradeoff between the tracking speed and the COG accuracy [2], an optimum α value of 2.0×10^{-3} is chosen in Section 4.4.

4.4. Transmission Performance

Making use of the synchronization technique, Fig. 7 shows the total channel BER performance of the 64-QAM-encoded, 11.25-Gb/s OOFDM signals for both the optical back-to-back configuration and 25-km MetroCor SMFs at an initial SCO of 0 ppm. A minimum BER of 3.3×10^{-4} for the 25-km SMF transmission is obtained, which is approximately three times lower than that measured in [15], where manual synchronization is used in a similar system configuration. In addition, in comparison with [15], the minimum optical power required for achieving a total channel BER of 1.0×10^{-3} is reduced by >3 dB. This strongly verifies the high accuracy of the synchronization technique. It should be noted that, in comparison with the optical back-to-back configuration, the observed better total channel BER performance for the 25-km MetroCor SMF case subject to received optical powers of >-12 dBm is due to the utilization of the negative chromatic dispersion MetroCor SMFs, as such fibers can compensate the positive transient frequency chirp associated with the DML [16]. On the other hand, as shown in Fig. 7, for both transmission configurations, when received optical powers are lower than -12 dBm, almost identical BER performances occur because the receiver thermal noise effect becomes a dominant factor limiting the minimum achievable BERs.

5. Complexity Comparisons

Table 1 shows complexity comparisons between the proposed synchronization technique, the conventional synchronization techniques using CPs [11]–[13], and the training sequence-based

synchronization technique [9]. To make fair comparisons between different techniques, Table 1 is calculated in real-valued signal generation/detection systems, in which both the STO and SCO effects are compensated. For the proposed synchronization technique, according to (1) and (2), there are $2L$ real multiplication operations and $3L$ addition operations for the synchronization profile generation utilizing parallel signal processing. In addition, for calculating COG and compensating for SCO, serial signal processing is also employed, which requires two real multiplication operations and $(L+2)$ addition operations. Finally, to ease hardware implementation of multiplication with different α values, the α parameter form is chosen to be 2^{-m}, with m being an integer number. By using such a α parameter form, the number of real multiplication operations is reduced to 2 for Gaussian windowing and SCO estimation. On the other hand, making use of the operation formulas presented in [9] and [11]–[13], a calculation procedure similar to that mentioned above is employed to calculate the complexity of these two conventional synchronization techniques, based on an assumption that parallel signal processing can be adopted for high-speed data transmission.

It can easily be seen in Table 1 that the proposed synchronization technique requires the lowest number of multiplication operations and is also free from the inverse tangent computation, while the CP-based synchronization technique [11]–[13] has the highest level of operation complexity because of the use of a maximum likelihood estimator, which requires complicated calculations of the log-likelihood function for estimating synchronization errors.

6. Conclusion

Accurate and simple OOFDM synchronization at 11.25 Gb/s and with the considerably improved system performance has been experimentally demonstrated in end-to-end real-time DML-based 25-km MetroCor SMF IMDD systems. Both the STO and SCO effects can be effectively compensated with the OOFDM synchronization technique. SCO compensation has been achieved, for the first time, with an accuracy of < 1 ppm for initial SCOs as large as 4000 ppm. The complexity of the proposed synchronization technique has also been discussed. The demonstrated synchronization technique has advantages of low complexity, fast tracking speed, high accuracy, and suitability for high-speed optical transmission.

References

[1] R. P. Giddings and J. M. Tang, "Experimental demonstration and optimization of a synchronous clock recovery technique for real-time end-to-end optical OFDM transmission at 11.25 Gb/s over 25 km SSMF," *Opt. Express*, vol. 19, no. 3, pp. 2831–2845, Jan. 2011.

[2] X. Q. Jin, R. P. Giddings, E. Hugues-Salas, and J. M. Tang, "Real-time experimental demonstration of optical OFDM symbol synchronization in directly modulated DFB laser-based 25 km SMF IMDD systems," *Opt. Express*, vol. 18, no. 20, pp. 21 100–21 110, Sep. 2010.

[3] S. C. J. Lee, F. Breyer, S. Randel, H. P. A. van den Boom, and A. M. J. Koonen, "High-speed transmission over multimode fiber using discrete multitone modulation," *J. Opt. Netw.*, vol. 7, no. 2, pp. 183–196, Jan. 2008.

[4] Y. Benlachtar, P. M. Watts, R. Bouziane, P. Milder, D. Rangaraj, A. Cartolano, R. Koutsoyannis, J. C. Hoe, M. Püschel, M. Glick, and R. I. Killey, "Generation of optical OFDM signals using 21.4 GS/s real time digital signal processing," *Opt. Express*, vol. 17, no. 20, pp. 17 658–17 668, Sep. 2009.

[5] C. J. Youn, X. Liu, S. Chandrasekhar, Y.-H. Kwon, J.-H. Kim, J.-S. Choe, K.-S. Choi, and E. S. Nam, "An efficient and frequency-offset-tolerant channel estimation and synchronization method for PDM CO-OFDM transmission," presented at the Eur. Conf. Optical Commun., Torino, Italy, 2010, Paper 4.06.

[6] N. Kaneda, Q. Yang, X. Liu, S. Chandrasekhar, W. Shieh, and Y.-K. Chen, "Real-time 2.5 GS/s coherent optical receiver for 53.3-Gb/s sub-banded OFDM," *J. Lightw. Technol.*, vol. 28, no. 4, pp. 494–501, Feb. 2010.

[7] D. Qian, T. T.-O. Kwok, N. Cvijetic, J. Hu, and T. Wang, "41.25 Gb/s real-time OFDM receiver for variable rate WDM-OFDMA-PON transmission," presented at the Optical Fibre Commun./Nat. Fibre Optic Eng. Conf., San Diego, CA, 2010, Paper PDPD9.

[8] T. M. Schmidl and D. C. Cox, "Robust frequency and timing synchronization for OFDM," *IEEE Trans. Commun.*, vol. 45, no. 12, pp. 1613–1621, Dec. 1997.

[9] M. Speth, S. Fechtel, G. Fock, and H. Meyr, "Optimum receiver design for OFDM-based broadband transmission—Part II: A case study," *IEEE Trans. Commun.*, vol. 49, no. 4, pp. 571–578, Apr. 2001.

[10] B. Yang, K. B. Letaief, R. S. Cheng, and Z. Cao, "Timing recovery for OFDM transmission," *IEEE J. Sel. Areas Commun.*, vol. 18, no. 11, pp. 2278–2291, Nov. 2000.

[11] J.-J. V. D Beek, M. Sandell, and P. O. Borjesson, "ML estimation of time and frequency offset in OFDM systems," *IEEE Trans. Signal Process.*, vol. 45, no. 7, pp. 1800–1805, Jul. 1997.

[12] M. Sandell, J.-J. V. D Beek, and P. O. Borjesson, "Timing and frequency synchronisation in OFDM systems using the cyclic prefix," in *Proc. Int. Symp. Synchronisation*, Essen, Germany, Dec. 1995, pp. 16–19.
[13] C.-C. Chang and C.-K. Wang, "High speed pilot-less sampling frequency acquisition for DMT systems," in *Proc. IEEE ISCAS*, 2005, vol. 5, pp. 4895–4898.
[14] D. Matic, T. A. J. R. M. Coenen, F. C. Schout, and R. Prasad, "OFDM timing synchronisation: Possibilities and limits to the usage of the cyclic prefix for maximum likelihood estimation," in *Proc. IEEE Veh. Technol. Conf.*, 1999, pp. 668–672.
[15] R. P. Giddings, X. Q. Jin, E. Hugues-Salas, E. Giacoumidis, J. L. Wei, and J. M. Tang, "Experimental demonstration of a record high 11.25 Gb/s real-time optical OFDM transceiver supporting 25 km SMF end-to-end transmission in simple IMDD systems," *Opt. Express*, vol. 18, no. 6, pp. 5541–5555, Mar. 2010.
[16] X. Q. Jin, R. P. Giddings, and J. M. Tang, "Real-time transmission of 3 Gb/s 16-QAM encoded optical OFDM signals over 75km SMFs with negative power penalties," *Opt. Express*, vol. 17, no. 17, pp. 14 574–14 585, Aug. 2009.